Effect of Polymer Ligand Molecular Weight on Polymer-Coated Nanoparticle Location in Block Copolymers

Bumjoon J. Kim,[†,‡] Glenn H. Fredrickson,[†,‡,§] and Edward J. Kramer*[,†,‡,§]

Department of Chemical Engineering, Materials Research Laboratory, and Department of Materials, University of California, Santa Barbara, California 93106

Received August 28, 2007; Revised Manuscript Received October 16, 2007

ABSTRACT: Gold nanoparticles (Au−PS) coated with an areal chain density Σ of end-attached polystyrene (PS) chains of different molecular weights (M_n) are added to a lamellar diblock copolymer of poly(styrene-*b*-2-vinylpyridine) (PS-*b*-P2VP) to determine the critical areal chain density Σ_C below which the Au−PS nanoparticles adsorb to the PS-*b*-P2VP interface. Gold nanoparticles coated by thiol end functional polystyrene homopolymers (PS−SH) with M_n ranging from 1.5 to 13 kg/mol are synthesized with various areal densities of PS−SH chains on the nanoparticle surface. The particles are incorporated into a PS-*b*-P2VP diblock copolymer with $M_n = 196$ kg/mol. The P2VP block has a more favorable interaction with a bare gold particle surface than does the PS block, and this interaction becomes important as the coverage of gold particles by PS−SH decreases, leading to adsorption of the Au−PS to the interface below a critical areal chain density Σ_C. Σ_C decreases from 3.1 to 0.9 chains/nm^2 as the M_n of PS−SH chains increases from 1.5 to 13 kg/mol, leading to a scaling relation, $\sum_C \sim R_g^{-1} \sim M_n^{-0.6}$, which is very different from the behavior expected for polymer chains tethered to a flat surface, $\sum_C \sim R_g^{-2} \sim M_n^{-1}$, where R_g is the radius of gyration of the end-attached chains. A simple scaling relationship, $\Sigma_C \sim ((R + R_g)/RR_g)^2$ that takes into account the high curvature of the Au nanoparticle core of radius R, is derived and is shown to describe the data very well. For $\Sigma \approx \Sigma_C$, there is a slight tendency for the larger particles within the particle size distribution to adsorb preferentially to the PS/P2VP interface, a tendency that can be qualitatively understood by the fact that the absorption free energy per particle is predicted to scale roughly as R^2.

Introduction

The addition of inorganic nanoparticles to block copolymers is potentially a route for the fabrication of novel functional materials such as photonic band gap materials,[1] highly efficient catalysts,[2] chemical and biological sensors,[3] and high-density magnetic storage media.[4] The domain structure of the block copolymer provides a template within which the inorganic nanoparticles can be organized. A number of experimental methods have been developed for incorporating inorganic nanoparticles into polymeric nanostructures.[5−21] However, the precise control of both the size and the spatial arrangement of inorganic nanoparticles within the block copolymer is a critical requirement for most applications.

Nanoparticles with an inorganic core can be synthesized in solution using organic ligands that bind to the particle surfaces at areal ligand densities that stearically stabilize the particles against coalescence.[22−25] After purification to remove the unattached ligands, such core−shell particles in solution can be combined with a block copolymer, permitting coassembly of the block copolymer and ligand-coated nanoparticles into films by slow solvent evaporation. Early experiments[10] used alkane thiol ligands on Au nanoparticles, while in later experiments short polymer thiols corresponding to one or more of the blocks of the block copolymer were employed,[11,14,15,17,26] making it easier to predict where in the block copolymer the polymer-coated nanoparticles would reside. To our knowledge, there have been no systematic attempts to vary the molecular weight of the attached polymer ligands in such a system even though this molecular weight might be expected to influence both the conditions for optimum particle synthesis and the final location of the nanoparticles in the solvent cast block copolymer film.

In most experiments, the particles are designed so that they will be fully wet by one of the blocks and thus will locate within that block domain. Recent experiments, however, have also focused on nanoparticles that preferentially adsorb to the interfaces between the blocks.[10,11,14,17] In two-phase, low molecular weight fluid systems, small particles that adsorb to the interfaces between the phases are well-known to have surfactant like properties, enabling, for example, the formation of stable "Pickering" emulsions.[27−29] "Jamming" of such particles at fluid−fluid interfaces can stabilize bicontinuous emulsions[30] and bicontinuous blends of immiscible polymers.[31] In lamellar block copolymers, nanoparticles that adsorb to the interfaces decrease the lamellar spacing at low particle volume fractions by virtue of their action as surfactants to decrease the interfacial tension and cause a transition to a fine scale bicontinuous domain structure at high particle volume fractions.[32]

Recent experiments have revealed several strategies of synthesizing nanoparticles that will adsorb at A−B block copolymer interfaces. Gold nanoparticles coated with a mixture of A and B ligands have been shown to segregate to the interface over a wide range of A fraction on the nanoparticle surface, if the ligands are free to diffuse on the Au surface.[11,33] AB random copolymer ligands are also effective in producing nanoparticles that adsorb on the interface, although in this case the A fraction must be approximately 0.5.[33] Both these methods require more synthesis steps than a third strategy, in which a Au nanoparticle that would preferentially bind to the B block is coated with an areal density of A thiol ligands too low to prevent contact with the B block if the particle adsorbs to the interface.[14]

In this paper, we generalize this simple procedure for controlling the location of PS-coated gold nanoparticles within

* To whom correspondence should be addressed. E-mail: edkramer@mrl.ucsb.edu.
† Department of Chemical Engineering.
‡ Materials Research Laboratory.
§ Department of Materials.

10.1021/ma701931z CCC: $40.75
Published on Web 12/18/2007

Table 1. Characteristics of Polymers Used in Present Study

list	$PS_{1.5}$−SH	$PS_{2.5}$−SH	$PS_{3.4}$−SH	$PS_{6.5}$−SH	PS_{13}−SH
M_n (kg/mol)	1.5	2.5	3.4	6.5	13
PDI	∼1.2	∼1.1	∼1.15	∼1.1	∼1.1
R_g (nm)	0.76	1.10	1.34	1.99	2.93

the lamellar PS-*b*-P2VP block copolymer domains by variation of a single parameter, the areal density of PS thiol ligands on the nanoparticles. P2VP acts as the B block, because of its strong adsorption to the Au surface.[34] Since we expect the critical areal chain density below which such particles adsorb to the interface to depend on the molecular weight of the PS thiol (PS−SH) ligands, we synthesized a series of these with number-average molecular weights (M_n) ranging from 1.5 to 13 kg/mol. In turn, the ligands were used in the syntheses of batches of Au nanoparticles 2−3 nm in Au diameter with various areal densities of ligands on their surfaces. We show that indeed the critical areal chain density Σ_C decreases as the M_n of the ligand increases but much less slowly than would be expected if Σ_C were to correspond to a mushroom to brush transition on a flat surface.[35,36] We propose a simple model that takes the curvature of the nanoparticle surface into account and show that it provides a reasonable fit to the data.

Experimental Section

Synthesis of Thiol-Terminated PS. A symmetric poly(styrene-*b*-2-vinylpyridine) (PS-*b*-P2VP) diblock copolymer with total molecular weight $M_n \sim 196\,500$ g/mol and a polydispersity index (PDI) of 1.11 (Polymer Source, Inc.) was used as the block copolymer template in which to investigate systematically the position of gold nanoparticles. Thiol-terminated PS (PS−SH), to be used as ligands to stabilize the Au nanoparticles during their synthesis, was synthesized by living anionic polymerization using benzene as solvent at 30 °C or using THF as solvent at −78 °C, as described previously.[12] The molecular masses M_n of the five different PS−SH were determined to be 1.5, 2.5, 3.4, 6.5, and 13 kg/mol by size exclusion chromatography calibrated with PS standards. The M_n and polydispersity of the PS−SH polymers are shown in Table 1. For convenience, these are labeled $PS_{1.5}$−SH, $PS_{2.5}$−SH, $PS_{3.4}$−SH, $PS_{6.5}$−SH, and PS_{13}−SH.

Synthesis of PS-Coated Au Nanoparticles. The synthesis of PS-coated Au nanoparticles was accomplished using a two-phase system[37] consisting of toluene and water by varying the initial mole feed ratio (f_{PS}) of PS ligands to (Au atoms + PS ligands). The polymer-coated gold particles were separated from unattached PS−SH by precipitation using a mixture of ethanol and toluene and concentrating the particles by centrifugation followed by membrane filtration (MWCO 30 000 dalton, Millipore, Inc.) using dimethyl formamide (DMF) as a solvent. To separate unattached $PS_{6.5}$−SH and PS_{13}−SH chains from their coated nanoparticles, a membrane with a larger pore size (MWCO 100 000 Da, Millipore, Inc.) was used. After the initial separation, the particles were redispersed in dioxane and washed by membrane filtration at least three more times to remove ungrafted ligands as well as any residual reducing agent. Finally, the particles filtered by the membrane were washed with methanol as reported before,[14] in this case, mainly for the purpose of easier removal of residual solvent from the gold particles.

Preparation of PS-*b*-P2VP/ Polymer-Coated Au Nanoparticle Composites. To prepare the PS-*b*-P2VP/ polymer-coated Au nanoparticle samples, a 1∼2 wt % block copolymer solution in dichloromethane was mixed with PS-coated gold nanoparticles to produce a dry weight fraction PS−Au/(PS−Au + PS-*b*-P2VP) of approximately 0.15−0.20. Samples containing gold particles with low areal chain density of PS−SH chains were prepared using a lower weight fraction of particles (<0.10) to prevent any morphological transition of the PS-*b*-P2VP matrix by nanoparticle surfactants.[32] Particle/block copolymer composites were prepared by solvent casting mixtures of PS-coated Au nanoparticles and PS-*b*-P2VP block copolymer in dichloromethane onto an epoxy substrate and then annealing under a saturated solvent atmosphere at 25 °C for at least a day. Dichloromethane is a relatively neutral solvent for PS and P2VP. All solvent in the sample was forced to evaporate very slowly over an additional day. Samples were subsequently dried in air overnight and further under vacuum for 4 h to make sure that no solvent is left in the sample. As a result of this procedure, a 5−20 μm thick film of nanoparticle/block copolymer composite was produced.

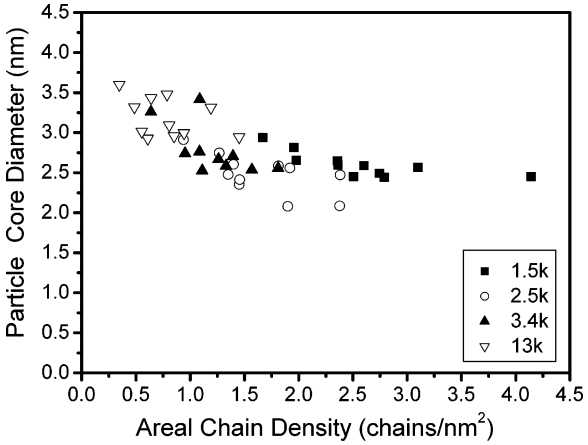

Figure 1. Au core diameter of particles coated by different PS−SH chains having M_n of 1.5, 2.5, 3.4, and 13 kg/mol is shown as a function of the areal chain density (Σ) of PS chains on Au nanoparticles.

Characterization. The sizes of the polymer-coated gold nanoparticles as well as the location of the PS-coated gold particles in the PS-*b*-P2VP were determined by transmission electron microscopy (TEM) using a FEI Tecnai G2 microscope operated at 200 kV. Gold nanoparticles were dissolved at a very low concentration in dichloromethane or THF. A thick carbon film (20−30 nm) on a TEM grid was dipped into the solution for a second, dried in air, and then examined by TEM. Samples of gold nanoparticle/block copolymer composites were prepared for cross-sectional TEM by microtoming epoxy-supported thick films into 25−40 nm thick slices and were then stained by exposing them to iodine vapor, which selectively stains the P2VP domains.

The gold core diameter distribution obtained as a histogram from TEM image analysis was used to calculate the average surface area per gold nanoparticle. Imaging conditions were varied systematically (a through focus series of images) to obtain accurate particle dimensions. Weight fractions of gold and polymer ligands were measured by thermal gravimetric analysis (TGA). The weight fractions of the polymer chains were converted into volume fractions using the density of the polymer (∼1.05 g/cm^3) and the density of the gold particles (∼19.3 g/cm^3). The number of polymer ligands per gold particle for various core−shell type particles divided by the average surface area of the gold particles gives the areal chain density of polymer ligands on the particle surface.

Results

The diameters of the Au core of the nanoparticles coated by the different PS−SH chains $PS_{1.5}$−SH, $PS_{2.5}$−SH, $PS_{3.4}$−SH, and PS_{13}−SH are shown in Figure 1 as a function of the areal density of the PS−SH chains (Σ) on the Au particle surface. The average particle core (Au) diameter for each Σ value was determined from TEM images by analyzing at least 300 particles using standard image analysis software (Image Pro). As Σ is decreased, the particles become larger and more polydisperse for a given polymer ligand. The particle core size is also slightly larger for the PS−SH ligands with larger M_n.

The areal chain densities of polymer ligands on the particle surface for various core−shell type particles were estimated based on the weight fractions of gold and polymer ligands obtained from elemental analysis and TGA. This information

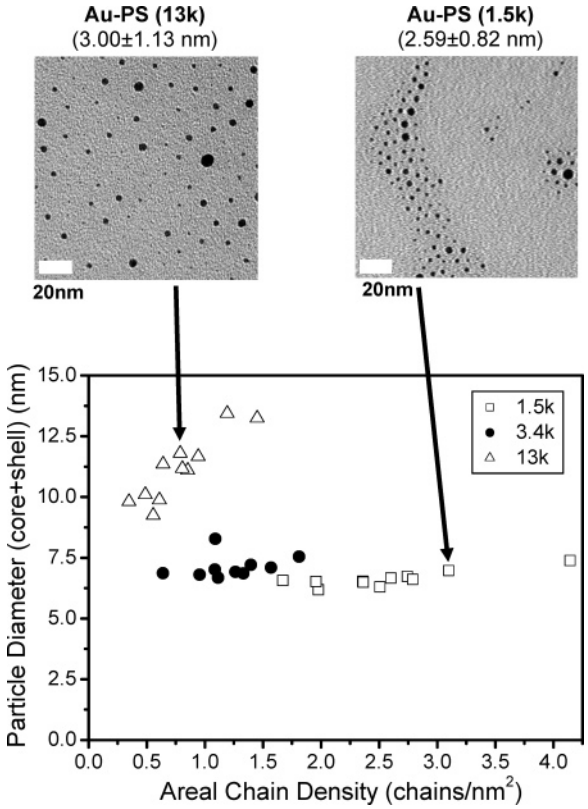

Figure 2. The particle diameter including the gold core and PS shell for PS−SH chains having M_n of 1.5, 3.4, and 13 kg/mol with a range of Σ values is shown in the graph. Two different TEM images represent the closely packed particles coated by PS−SH of 13 and 1.5 kg/mol, respectively, on carbon film-coated TEM grids. PS shell thickness increases significantly as the M_n of PS−SH chains increases from 1.5 to 13 kg/mol.

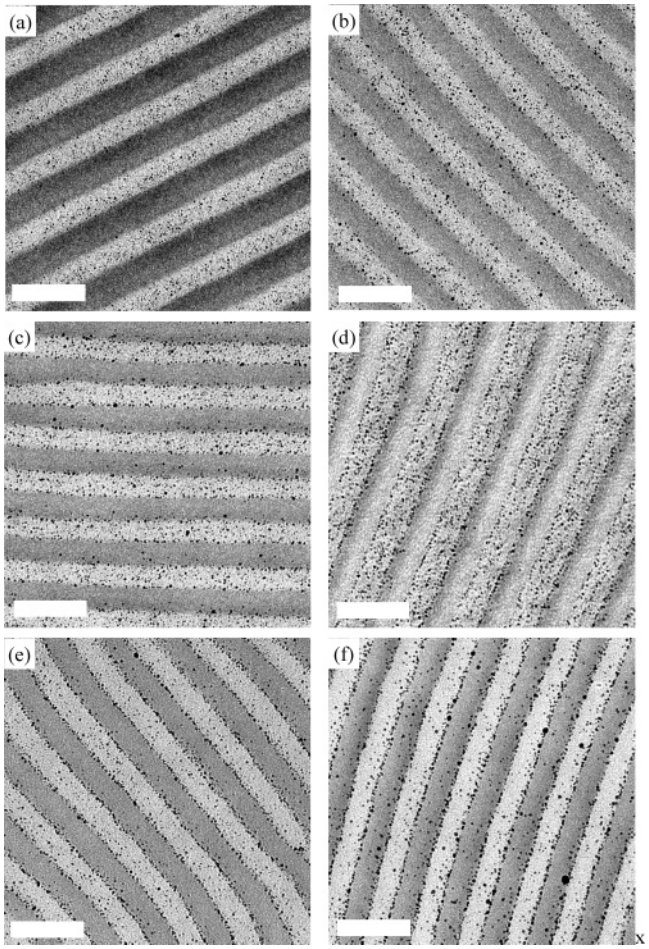

Figure 3. Cross-sectional TEM images of PS-*b*-P2VP block copolymer containing PS-coated gold nanoparticles whose surfaces are covered with various areal chain densities of $PS_{2.5}$−SH chains (M_n = 2.5 kg/mol): (a) 2.38 chains/nm^2, (b) 1.92 chains/nm^2, (c) 1.81 chains/nm^2, (d) 1.47 chains/nm^2, (e) 1.40 chains/nm^2, and (f) 0.92 chains/nm^2. Scale bar is 100 nm.

also allows the average polymer shell thickness on each set of Au particles to be determined. The estimated mean particle diameter including both the Au core and the polymer shell is shown in Figure 2 for various PS−SH chains at different Σ values. Since the weight fraction of polymer ligands in these polymer-coated particles decreases as Σ decreases, the PS shell thickness becomes smaller. The particle diameter coated with PS_{13}−SH is much larger than that coated with $PS_{1.5}$−SH as shown in Figure 2. The TEM images in Figure 2 provide qualitative support for the increase in shell thickness, as can be seen in the insets in Figure 2. The particle core diameter (3.00 ± 1.13 nm) of the PS_{13}−SH-coated sample (shown in Figure 2a) is not much different from that of the $PS_{1.5}$−SH-coated (2.59 ± 0.82 nm) one, but the distance between particle cores dispersed on the carbon film on the TEM grid is significantly larger for PS_{13}−SH-coated than for $PS_{1.5}$−SH-coated particles, which indicates that the PS shell on the Au particle core coated by PS_{13}−SH is much thicker.

Figure 3 shows cross-sectional TEM images of PS-*b*-P2VP block copolymer containing PS-coated gold nanoparticles whose surfaces are covered with various Σ values of $PS_{2.5}$−SH. To produce various particles with areal chain densities ranging from 2.38 to 0.92 chains/nm^2, the initial mole feed ratio of PS ligands to (Au atoms + PS ligands), f_{PS}, is varied from 0.3 to 0.06. The darker gray regions in Figure 3 correspond to P2VP domains, since P2VP is selectively stained by the iodine vapor treatment used to provide contrast. PS domains appear as light gray, and the Au cores of the nanoparticles are evident as small black dots. From Figure 3a, it is clear that the particles are located near the center of the PS domains (lighter regions) when the $PS_{2.5}$−SH areal chain density is relatively high, 2.38 chains/nm^2. As Σ decreases, the particles are distributed roughly equally between the center of the PS domain and the interface as seen in panels b and c of Figure 3, corresponding to 1.8−1.9 chains/nm^2. As the $PS_{2.5}$−SH areal chain density on the Au particles decreases further from 1.81 to 1.40 chains/nm^2 (Figure 3e), most nanoparticles are clearly segregated along the interface between PS and P2VP, and at Σ = 0.92 chains/nm^2 (Figure 3f), virtually all nanoparticles are at the PS/P2VP interface. Histograms of the particle locations for these samples are shown in Figure 4, and they serve to quantitatively reinforce the qualitative impressions from examining the TEM micrographs. While the TEM micrographs provide direct evidence of particle location as a function of the areal chain density, errors in the particle distribution within a polymer block domain may be caused by the tilt of the lamellar interfaces relative to the TEM beam direction so that the interfaces appear broader and the domains are narrow in the projected image. Care was taken to reduce such errors both by carefully tilting the sample so as to minimize the interface width and by analyzing a large number of particles (at least 500 particles) collected from different samples at given areal chain density. These data are used to produce the histograms in Figure 4. Our rationale for this behavior is that nanoparticles with relatively low $PS_{2.5}$−SH areal chain densities do not fully shield the Au nanoparticle surface from interacting with the P2VP block of the PS-*b*-P2VP matrix, since there is a

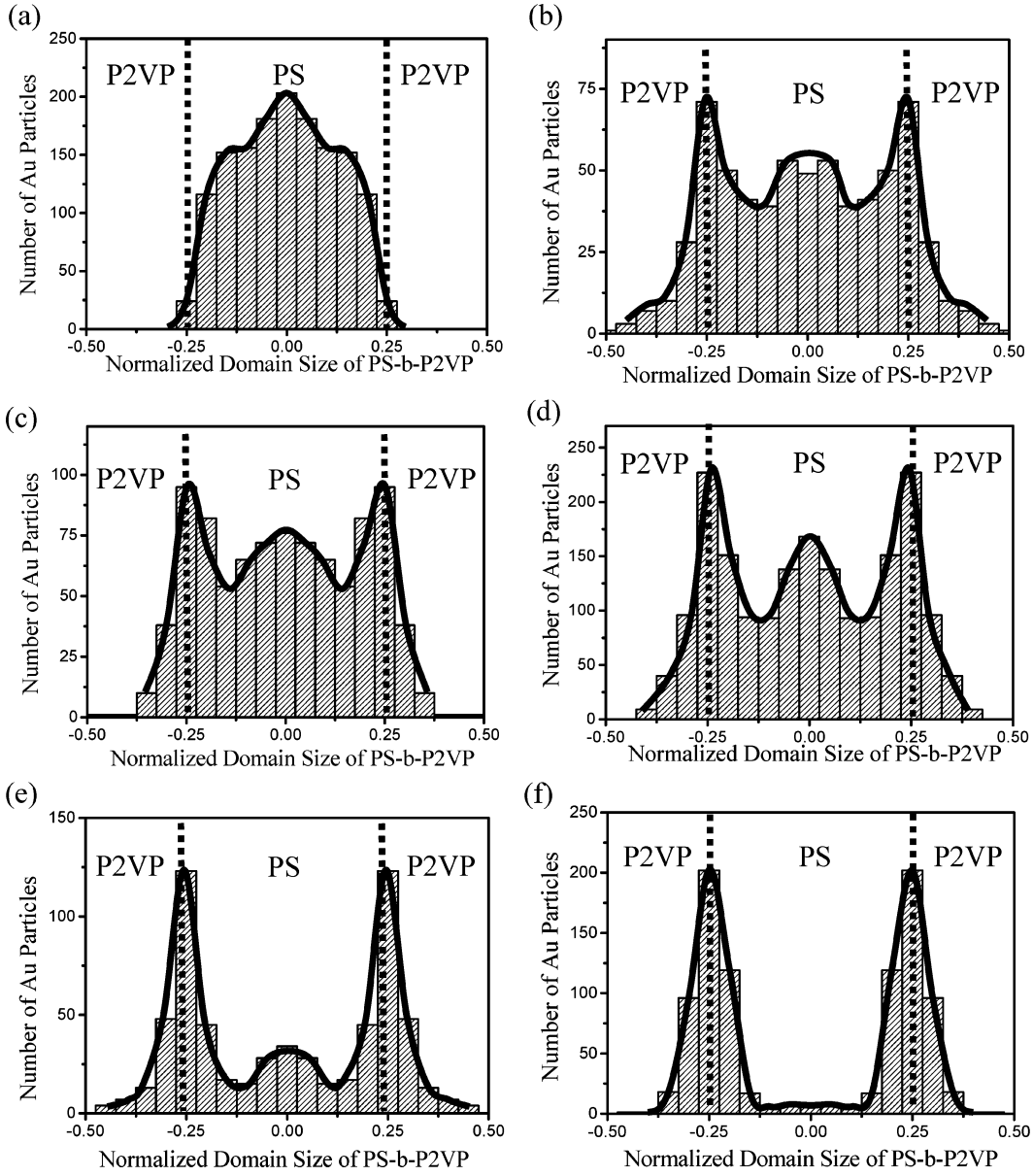

Figure 4. Histograms of particle positions from the TEM micrographs in Figure 3: (a) 2.38 chains/nm^2, (b) 1.92 chains/nm^2, (c) 1.81 chains/nm^2, (d) 1.47 chains/nm^2, (e) 1.40 chains/nm^2, and (f) 0.92 chains/nm^2. Interface of the PS domain is at −0.25 and +0.25, and data are averaged at a given position relative to zero, i.e., number of particles at −0.2 = (number of particles at −0.2 + number of particles at +0.2)/2.

favorable interaction between gold and P2VP and the PS/gold interaction is relatively weaker. The favorable interaction between gold surface and P2VP has been reported by other research groups[34,38,39] and was confirmed by our model experiment,[14] where a layered structure of lamellar dPS-*b*-P2VP block copolymer consisting of a surface half-lamella of dPS on the surface and a half-lamella of P2VP on the Au substrate is observed.

The histogram in Figure 4a clearly shows the occurrence of a single peak in the particle density distribution at the center of the PS domain when particles have relatively high areal chain density of 2.38 chains/nm^2, where the unfavorable interaction between the PS ligands of the particle surface and the P2VP domain is dominant. Interestingly, in the intermediate Σ regime, the particle density distribution has the three different peaks, one at the center of the PS domain and the other two at the PS/P2VP interface, and upon further decrease in Σ, the particles are strongly segregated to the PS/P2VP interface and the peak at the PS center disappears. This trend is consistent with the recent theoretical predictions (simulation results) by Pryamitsyn and Ganesan.[40] We speculate that the three different peaks in the particle distribution at the intermediate Σ, such as 1.81 and 1.47 chains/nm^2, result from the variation in the enthalpic interaction of various polymer-coated particles with the P2VP block, which is influenced by the distribution of the number of PS chains on the nanoparticles. We will discuss this issue further in the next section.

The trend in the dramatic change of the particle location from the center of PS domain to the PS/P2VP interface is universally observed for PS−Au particles regardless of M_n. Cross-sectional TEM images of PS-*b*-P2VP block copolymer containing gold nanoparticles coated by the shortest PS ligands, $PS_{1.5}$−SH (M_n = 1.5 kg/mol), are shown in Figure 5. Particles with Σ = 3.97 chains/nm^2 are located within the PS domain, while most gold particles with Σ = 2.36 chains/nm^2 are shown to be segregated to the PS/P2VP interface. Histograms corresponding to the TEM images reflecting this transition of particle location in the PS-*b*-P2VP template are also shown in Figure 5.

Figure 6 shows cross-sectional TEM images of the gold particles coated with the longest PS ligands, PS_{13}−SH (M_n =

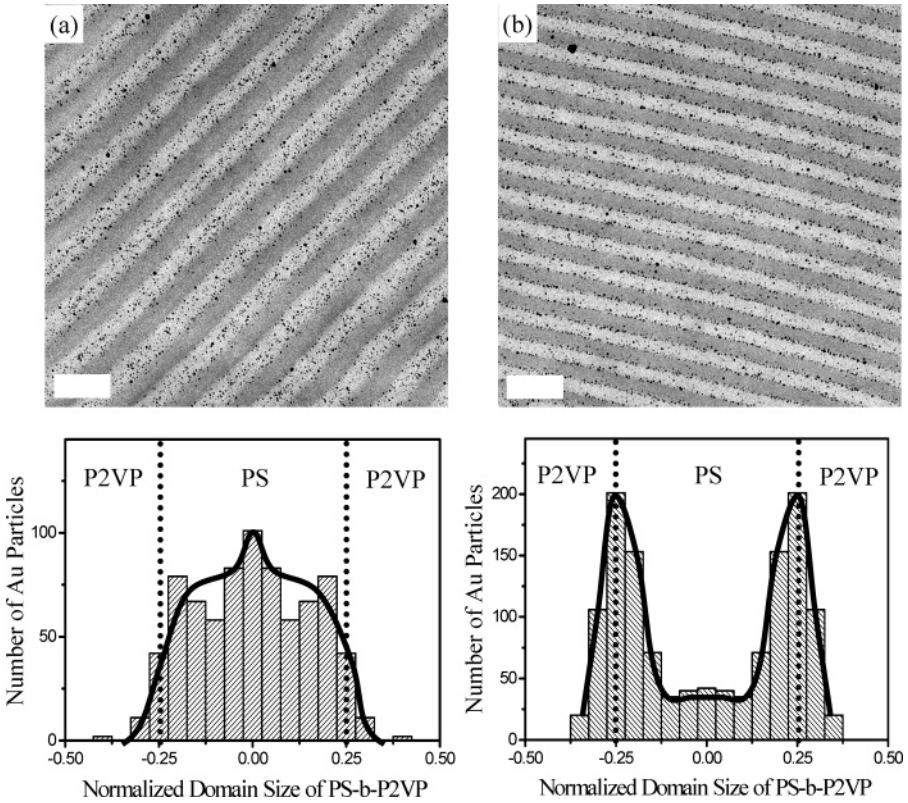

Figure 5. Cross-sectional TEM images of PS-*b*-P2VP block copolymer containing PS-coated gold nanoparticles whose surfaces are covered with two different Σ values of $PS_{1.5}$−SH chains (M_n = 1.5 kg/mol): (a) 3.97 chains/nm^2 and (b) 2.36 chains/nm^2. Scale bar is 100 nm. Histograms of particle positions describe the particle distribution from the corresponding TEM micrographs. Interface of the PS domain is at −0.25 and +0.25.

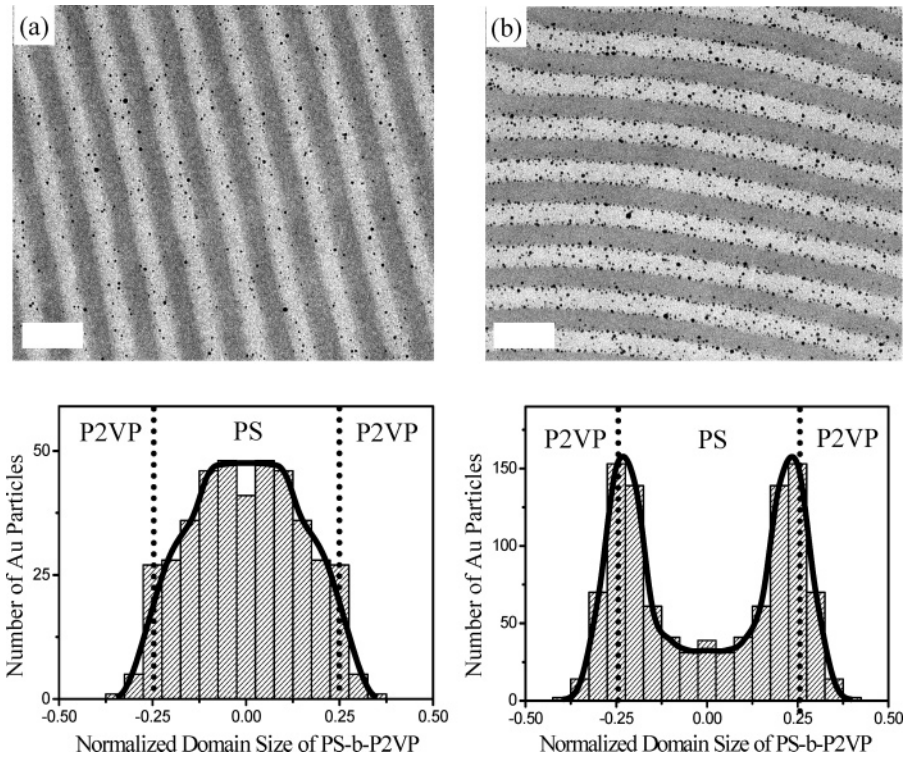

Figure 6. Cross-sectional TEM images and their corresponding histograms of PS-*b*-P2VP block copolymer containing PS-coated gold nanoparticles whose surfaces are covered with two different Σ values of PS_{13}−SH chains (M_n = 13 kg/mol): (a) 1.22 chains/nm^2 and (b) 0.83 chains/nm^2. Scale bar is 100 nm.

13 kg/mol), within a PS-*b*-P2VP block copolymer. Two different particles with areal chain densities of (a) 1.22 chains/nm^2 and (b) 0.83 chains/nm^2 are used. The location of particles shifts from the PS domain to the PS/P2VP interface as Σ decreases from 1.22 to 0.83 chains/nm^2. Of particular interest is that the critical areal chain density (Σ_C) for the transition of particle location in the case of PS_{13}−Au nanoparticles is found to be 0.9 chains/nm^2, which is much lower than Σ_C (∼3.1 chains/nm^2) for $PS_{1.5}$−Au nanoparticles. This observation indicates that fewer PS_{13}−SH chains are required to cover the Au particle

surface fully. Below the TEM micrographs, histograms derived from them show the location of the PS_{13}−Au nanoparticles.

The particle density shown in Figure 6a is not high, since a large amount of PS_{13}−SH-coated gold particles cannot be accommodated in the PS-*b*-P2VP template (M_n = 196 kg/mol) without macrophase separation. The PS_{13}−SH-coated gold particles that are located in the PS domain coexist with large regions of aggregated nanoparticles present at even relatively low volume fraction of the particles (∼0.15). There is evidently a phase coexistence between a macrophase that is highly enriched in particles and a lamellar mesophase with a much lower particle concentration. At comparable particle volume fractions, a corresponding macrophase separation of gold particles is not observed in the PS-*b*-P2VP block copolymer template (M_n = 196 kg/mol) containing gold particles coated with $PS_{1.5}$−SH, $PS_{2.5}$−SH, and $PS_{3.4}$−SH having lower M_n. We believe that the macrophase separation in the sample containing gold particles coated by PS_{13}−SH (M_n = 13 kg/mol) at a relatively lower particle volume fraction is caused by the increased tendency toward the immiscibility between particles and PS-*b*-P2VP templates due to increased particle size. Since the PS block chains are tethered chains with one end fixed at the PS/P2VP interfaces, the mixing of such tethered PS chains with PS-coated particles gives rise to a significant conformational entropy penalty in order to mix the PS-coated particles with the PS block chains. The penalty will increase as the particle size becomes larger. A similar trend is observed for blends of diblock copolymer and homopolymers. Addition of a homopolymer of increasing M_n to the lamellar diblock copolymer results in a decreasing volume fraction of the homopolymer that can be added before macrophase separation occurs.[41,42]

Discussion

The size effect of selective particles in a block copolymer matrix has been investigated theoretically[43,44] and experimentally,[10,17,45] showing that the particle size is one of the major factors that determines the particle location within a block copolymer matrix. In situations where particles are densely coated by only A homopolymers, so that their unfavorable interaction with the B block of A-*b*-B block copolymer is dominant, simulations and some experiments[10,17] suggest that smaller particles tend to be selectively located not only in the A block but also along the A/B interfaces while larger particles are found to be near the center of A polymer domains to minimize the entropic penalty of chain stretching. On the other hand, experiments with longer polymer ligands on nanoparticles of constant size show Gaussian distributions of nanoparticles positioned at the center of the A domain regardless of the lamellar spacing of the block copolymer, which is at odds with the predictions of simulations that find a tendency for placement near the interface when the A domain size increases.[45] While the behavior of selective particles has been studied intensively, the effect of the size of nanoparticles that are attracted enthalpically to the interface has not been investigated experimentally. In contrast to the case where particles selective for one domain should be preferentially attracted to the domain center due to entropy, when nanoparticles are enthalpically attracted to the interface, larger particles are expected to be preferentially segregated there, since the adsorption energy of particles at the interface is proportional to the square of the nanoparticle radius. The adsorption energy of gold nanoparticles at the interface between PS and P2VP blocks (E_a) can be expressed approximately by the following equation:[46] where

$$E_a/k_BT = (\pi R^2 \gamma_{PS-P2VP}/k_BT)^*(1 - |\mathrm{Cos}(\theta)|)^2$$

$$|\mathrm{Cos}(\theta)| = \frac{|\gamma_{PS-NP} - \gamma_{P2VP-NP}|}{\gamma_{PS-P2VP}} \quad (1)$$

where R is the radius of nanoparticle, and $\mathrm{Cos}(\theta)$ is the ratio of the difference in interfacial tension between nanoparticles and the PS and P2VP blocks to that between PS and P2VP. Equation 1, however, ignores the effects of particle radius on the conformational entropy of the block copolymer. In the intermediate Σ regime where the particles are located both at the PS/P2VP interface and near the center of PS domain, the interplay between entropic and enthalpic effects of particle size on determining the particle location could be important.

To investigate the phenomena systematically, the particle core diameter as a function of the particle location in the normalized PS-*b*-P2VP domain is obtained from TEM image analysis of at least 500 particles for each histogram in Figure 7. These histograms summarize the particle size distribution as a function of the particle location for the PS-*b*-P2VP block copolymer containing PS-coated gold nanoparticles whose surfaces are covered with various Σ of $PS_{2.5}$−SH chains (M_n = 2.5 kg/mol): (a) 2.38 chains/nm^2, (b) 1.92 chains/nm^2, (c) 1.47 chains/nm^2, and (d) 1.40 chains/nm^2. At Σ = 2.38 chains/nm^2, where all particles are dispersed in the PS domain as shown in Figures 3a and 4a, the mean particle diameter ($\langle d \rangle$ = 2.7 nm) is larger near the PS center than closer to the PS/P2VP interface ($\langle d \rangle$ = 2.1 nm), as shown in Figure 7a. Due to the unfavorable interaction between the P2VP blocks and PS ligands on the particle surface, no segregation of particles at the interface is observed at this value of Σ. Since larger particles cause a larger entropy penalty of the PS block of PS-*b*-P2VP in order to accommodate the particles in the PS brush near the interface of the PS domain, the larger particles tend to be located nearer to the middle of PS domain between the two PS brushes, in rough agreement with the simulation results of Thompson et al.[43]

The particle size distribution changes as Σ decreases, as some fraction of the particles become bound to the interface. At an intermediate Σ of 1.92 chains/nm^2, the particle size at the PS/P2VP interface becomes larger than that near the center of PS domain. While the mean particle core diameter located at the PS/P2VP interface is 2.95 nm, the mean particle core diameter at the center of the PS domain is 2.5 nm. If two different particles located at the PS/P2VP interface and the PS center are assumed to have the same volume fraction of PS chains on the particle surface, the mean particle diameter including the PS shell is 7.28 nm for particles at the interface and the mean particle diameter (core + shell) is 6.18 nm at the center of the PS domain. The difference in the mean particle size should produce a ratio of adsorption energy of 1.4 from eq 1. However, even though the maximum value of the mean particle diameter $\langle d \rangle$ is observed at the PS/P2VP interface, $\langle d \rangle$ at the center of PS domain is slightly larger than $\langle d \rangle$ at other positions within the PS domain, i.e., there are two maxima in $\langle d \rangle$, one at the PS/P2VP interface and a smaller one at the PS domain center. The small maximum at the PS domain center is consistent with the results for the high areal chain density particles (Figure 7a). Therefore, we conclude that in the intermediate Σ regime both the entropic and the enthalpic effects of particle size combine to determine the particle distribution within the block copolymer based on its size, producing the maximum $\langle d \rangle$ at the PS/P2VP interface due to the strongly increasing adsorption energy at the interface with d. The same trend is observed for the particle distribution at lower Σ values of 1.47 and 1.40 chains/nm^2 shown

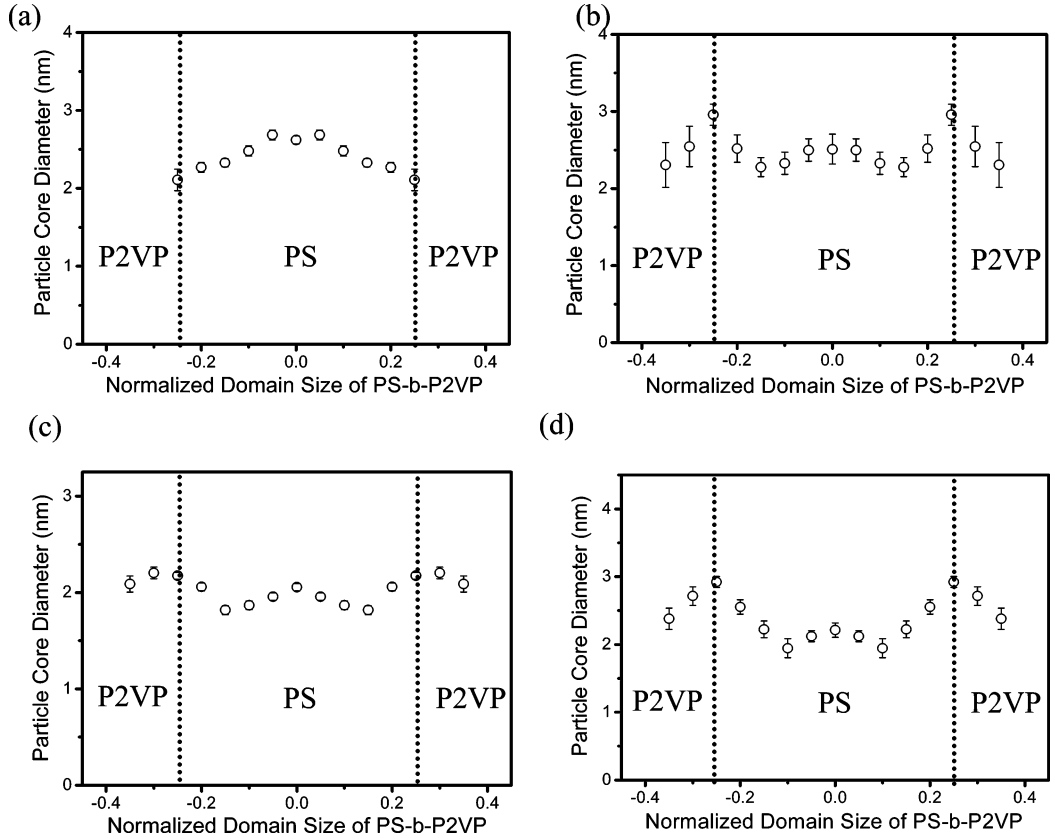

Figure 7. Histogram of the mean particle diameter is shown as a function of particle location in PS-*b*-P2VP. Particle diameter is obtained from image analysis of TEM images with at least 500 particles of PS-*b*-P2VP block copolymer containing PS-coated gold nanoparticles whose surfaces are covered with various areal densities Σ of $PS_{2.5}$−SH chains (M_n = 2.5 kg/mol): (a) 2.38 chains/nm^2, (b) 1.92 chains/nm^2, (c) 1.47 chains/nm^2, and (d) 1.40 chains/nm^2 corresponding to the TEM micrographs and particle position histograms in Figures 3a−e and 4a−e, respectively. For example, the mean particle diameter at the normalized particle location (x) = 0 is obtained by averaging the particles located between x = -0.025 and 0.025.

in panels c and d of Figure 7. A small peak in ⟨d⟩ is seen at the PS domain, but ⟨d⟩ is always a maximum at the PS/P2VP interface.

To further illustrate the generality of the particle distribution as a function of ⟨d⟩ found for gold particles coated with $PS_{2.5}$−SH in Figure 7, gold particles coated two different ligands, $PS_{1.5}$−SH (M_n = 1.5 kg/mol) and $PS_{3.4}$−SH (M_n = 3.4 kg/mol), with intermediate Σ values close to Σ_C are chosen. The histograms of ⟨d⟩ corresponding to the $PS_{1.5}$−SH-coated particles (Σ = 2.6 chains/nm^2) and $PS_{3.4}$−SH-coated particles (Σ = 1.6 chains/nm^2) are shown in panels (c) and (d) of Figure 8 below the corresponding histograms, (a) and (b), of the particle location distribution. The particle size distribution as a function of particle location for both $PS_{1.5}$−Au and $PS_{3.4}$−Au nanoparticles is consistent with that observed for the $PS_{2.5}$−Au nanoparticles. At the PS/P2VP interface, ⟨d⟩ has a maximum value of 2.7−2.8 nm while between the PS/P2VP interface and the PS center ⟨d⟩ has a minimum value of 2.2−2.3 nm. Nevertheless, by comparing panels (e) and (f) of Figures 8, the histograms of particle diameter for those particles adsorbed at the interface with histograms of particle diameter for those particles in the center of the PS domain, we realize that many particles with a given diameter are at the interface while others with the same diameter are in the middle of the PS domain. The reasons for this result are considered below.

We define (and determine) the critical areal chain density (Σ_C) as the Σ at which approximately one-half of the particles are at the PS/P2VP interface and the remaining half are in the PS block. For example, to determine Σ_C for $PS_{3.4}$−SH (M_n = 3.4 kg/mol)-coated gold particles, the particle fractions located at the PS/P2VP interface (f_I) for various Σ values are obtained from TEM image analysis as shown in Figure 9b. A value of Σ = Σ_C ∼ 1.6 chains/nm^2 is found to produce an $f_I \approx 0.5$ for $PS_{3.4}$−SH-coated particles. On the other hand, the particle density profile of $PS_{3.4}$−Au particles at various Σ values provides a means to doublecheck if our selection for Σ_C is reasonable. We believe that the primary reason for the different behavior of various particles, in addition to the effects of particle diameter discussed above, is the fact that the average number ⟨n⟩ of PS−SH chains bound to these small Au particles is quite small. For example, $PS_{3.4}$−SH-coated gold particles that have Σ = 1.56 chains/nm^2 have ⟨n⟩ = 32. If the number of PS−SH chains per particle follows a Poisson distribution, which seems a reasonable assumption at all but the largest Σ, it implies that the standard deviation corresponds to n ≈ 6 chains and thus a significant fraction of the particles will have more than 38 (Σ = 1.87 chains/nm^2) and less than 26 chains (Σ = 1.28 chains/nm^2). Therefore, considering the size distribution of the particle diameter, the fraction of particles that have Σ less than Σ_C (=1.6 chains/nm^2) for a given average value of Σ may be calculated, and this fraction yields f_I. The details of this calculation are given in the Appendix. The calculated results are represented by filled symbols. A sigmoidal curve is fit to these values and is plotted in Figure 9b. The agreement between unfilled and filled symbols indicates that Σ_C ∼ 1.6 chains/nm^2 for $PS_{3.4}$−SH-coated particles is a reasonable choice. Following the same method for $PS_{2.5}$−SH-coated gold particles, Σ_C = 1.85 chains/nm^2 is found, yielding an f_I (filled circles) that gives excellent agreement with the experimental data (open squares) as shown in Figure 9a.

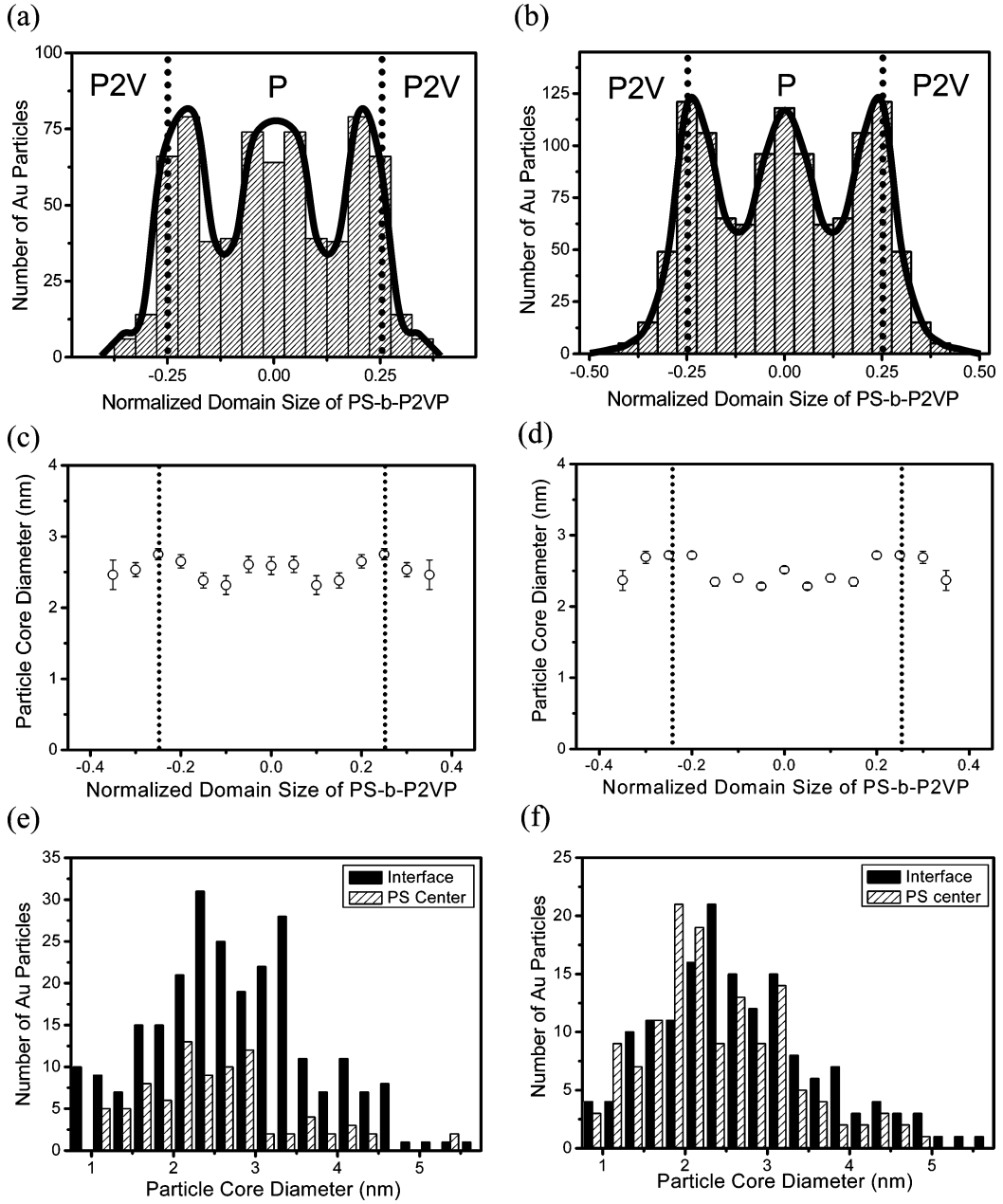

Figure 8. Two histograms describe particle distributions obtained from TEM images of PS-*b*-P2VP block copolymer containing PS-coated gold nanoparticles with intermediate Σ values close to Σ_C, where particles are located both at the center of PS domain and the interface between PS and P2VP blocks. (a) Gold particles are coated by $PS_{1.5}$−SH chains ($\Sigma = 2.6$ chains/nm^2). (b) Gold particles are coated by $PS_{3.4}$−SH chains ($\Sigma = 1.6$ chains/nm^2). The corresponding histograms (panels c and d) of average particle diameter as a function of particle location in PS-*b*-P2VP are shown . The particle diameter distributions at two different locations, in the middle of PS domain ($x = 0$) and at the PS/P2VP interface ($x = -0.25$ and 0.25), are chosen to produce the histograms of average particle diameter for the corresponding $PS_{1.5}$−Au and $PS_{3.4}$−Au particles (panels e and f).

Figure 10 represents a "phase diagram" for the location of PS−SH-coated gold particles in the PS-*b*-P2VP system expressed in the coordinates of the molecular weight (M_n) and mean areal density of PS−SH chains (Σ). The phase diagram summarizes the location of gold nanoparticles coated by PS−SH chains with M_n values of 1.5 kg/mol (squares), 2.5 kg/mol (circles), 3.4 kg/mol (triangles), and 13 kg/mol (inverse triangles) within the PS-*b*-P2VP block copolymer (M_n= 196 kg/mol). As Σ of PS−SH chains decreases, the figure shows that particles are seen at the center of the PS domains at large Σ, approximately evenly distributed between the PS domain centers and the PS/P2VP interface at smaller Σ, and entirely at the PS/P2VP interface at the lowest Σ for gold particles coated by PS−SH chains with various M_n. As Σ of the PS−SH chains decreases, thus exposing the bare surface of gold particles to the surrounding polymer, the favorable interaction between P2VP and the gold particle surface plays a more important role in controlling the particle location, and the particle location shifts from the PS domain (filled symbols) to the PS/P2VP interface (open symbols). The half-filled symbols represent the conditions where the particles are located both at the PS/P2VP interface and near the PS center. The light yellow filled area in the graph corresponds to the conditions for the majority of the particles being bound to the PS/P2VP interface.

The value of Σ_C decreases from 3.1 to 0.9 chains/nm^2 as the M_n of the PS−SH chains increases from 1.5 to 13 kg/mol. This decrease indicates that fewer PS−SH chains are required to shield the Au particle surface from interacting with the P2VP chains as the length of the PS−SH chain on the nanoparticle surface increases. The critical areal chain density (Σ_C) is plotted

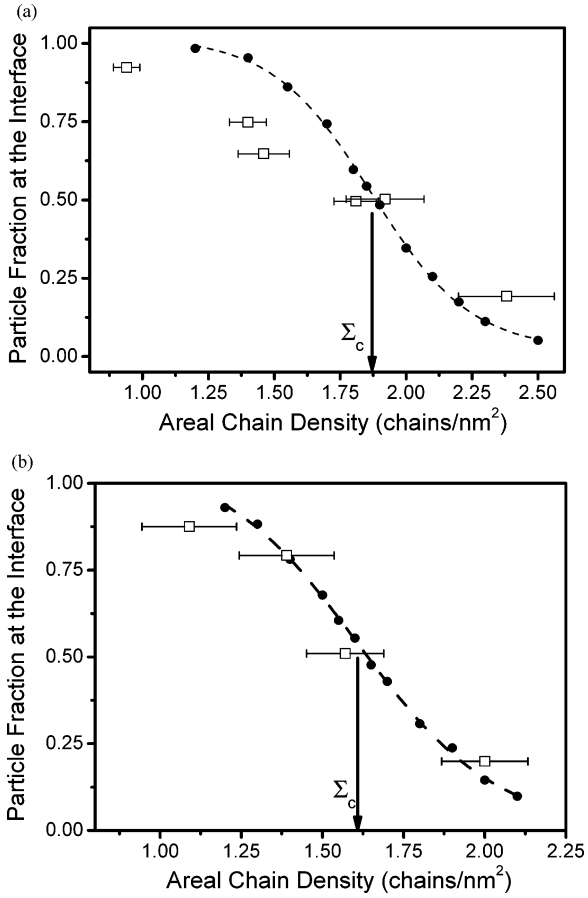

Figure 9. Particle fraction located at the PS/P2VP interface (f_I) as a function of Σ: (a) Au particles coated by $PS_{3.4}$−SH chains, and (b) Au particles coated by $PS_{2.5}$−SH chains. Unfilled squares represent experimental values of f_I obtained from different sets of particles having various average values of Σ. In comparison, filled circles represent f_I calculated using the procedure given in the text for the sample of (a) $PS_{2.5}$−Au ($\Sigma_C = 1.81$ chains/nm^2) and (b) $PS_{3.4}$−Au ($\Sigma_C = 1.57$ chains/nm^2). Dotted lines show sigmoidal curves fit to the filled symbols.

as a function of the M_n of the PS−SH chains in Figure 11a. Forcing a linear fit to the data on this log−log plot results in the following scaling relation, $\Sigma_C \sim M_n^{-0.60}$, between Σ_C and M_n. One expects that the radius of gyration R_g of the short PS ligands must be important in shielding the Au particles from contact with the P2VP block, but since these chains are very short, one cannot use the usual expressions for R_g ($[R_g^2]_\infty = Na^2/6$, where N is the degree of polymerization and a is the statistical segment length) that are valid in the long chain limit. Instead, the wormlike chain model is used here to estimate the actual radius of gyration (R_g) of the short PS−SH chains. The correction factor from the wormlike chain model ($f_{corr} = R_g^2/[R_g^2]_\infty$) can be calculated by the following equation:[47,48]

$$f_{corr} = 1 - \frac{1}{3}\left(\frac{l_P}{L}\right) + 6\left(\frac{l_P}{L}\right)^2 - 6\left(\frac{l_P}{L}\right)^3\left(1 - \exp\left(\frac{l_P}{L}\right)\right) \quad (2)$$

where l_P is the persistence length (=0.89 nm) for PS and L is the contour length of the chain. The calculated values of R_g of the PS−SH chains are given in Table 1. Figure 11b represents the Σ_C values in terms of the R_g values of all PS−SH chains, producing a scaling relation $\Sigma_C \sim R_g^{-0.96}$. This result is very different from what would be expected on a flat surface. If the polymer chains were tethered onto a flat surface, the dependence of the critical areal chain density (Σ_C) on the M_n of polymer chains is expected to be $\Sigma_C \sim M_n^{-1} \sim R_g^{-2}$ at high M_n, since

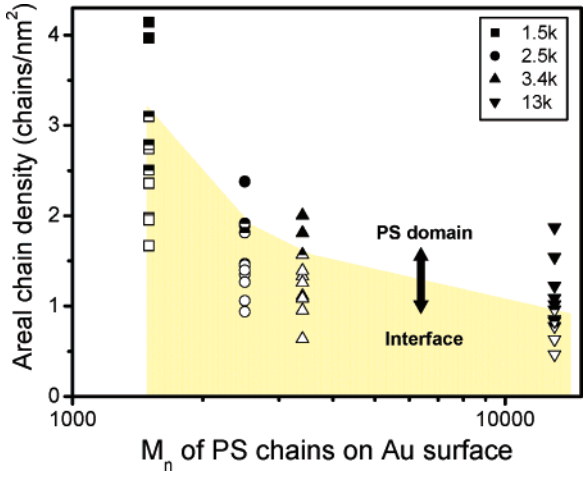

Figure 10. Phase diagram showing the location of PS−SH-coated gold particles in the PS-*b*-P2VP block copolymer expressed in terms of the coordinates of molecular weight (M_n) and areal density of PS−SH chains (Σ). The phase diagram summarizes the location of gold nanoparticles coated by PS−SH chains with M_n of 1.5 kg/mol (squares), 2.5 kg/mol (circles), 3.4 kg/mol (triangles), and 13 kg/mol (inverse triangles) within the PS-*b*-P2VP template ($M_n = 196$ kg/mol). As Σ of PS−SH chains decreases, the particle location shifts from the PS domain (filled symbols) to the PS/P2VP interface (open symbols). The half-filled symbols represent the conditions where the particles are located both at the PS/P2VP interface and near the PS domain center.

the area of the flat surface occupied by a single polymer chain at the mushroom to brush transition is proportional to R_g^2. However, since the particle core radius is comparable to the radius of gyration of the polymer chain tethered onto the particle surface, the gold particle surface is highly curved while the single chain stretching criterion is strictly applicable only for a brush on a flat surface. Therefore, the behavior of PS chains on the particle surface is expected to be very different from that on the flat surface. A somewhat more realistic model is required to understand the behavior of polymer brushes on a curved gold surface and to compute a transition areal chain density that corresponds to close packing of these short polymer ligand coils on a curved gold surface.

Consider a particle of radius R with some number n of grafted PS chains, each with a degree of polymerization N. We assume that the critical areal chain density (Σ_C) at which the transition from bulk to interfacial localization of particles occurs is

$$\Sigma_C \equiv \frac{n_C}{4\pi R^2} \quad (3)$$

where n_C is the corresponding critical number of grafted chains. If the particles were very large, and the surface locally flat on the scale of R_g, then Σ_C could be estimated by the threshold to mushroom−brush transition, where a PS brush is just enough to prevent the penetration of P2VP chains of PS-*b*-P2VP polymers into the PS shell on the gold surface.

$$\Sigma_C \sim \frac{1}{R_g^2} \sim \frac{1}{N} \quad (4)$$

For chains grafted to a particle with radius R comparable to R_g, a coverage based on the radius of the particle plus PS shell coating can be expressed as follows:

$$\Sigma' \equiv \frac{n}{4\pi(R+h)^2} \quad (5)$$

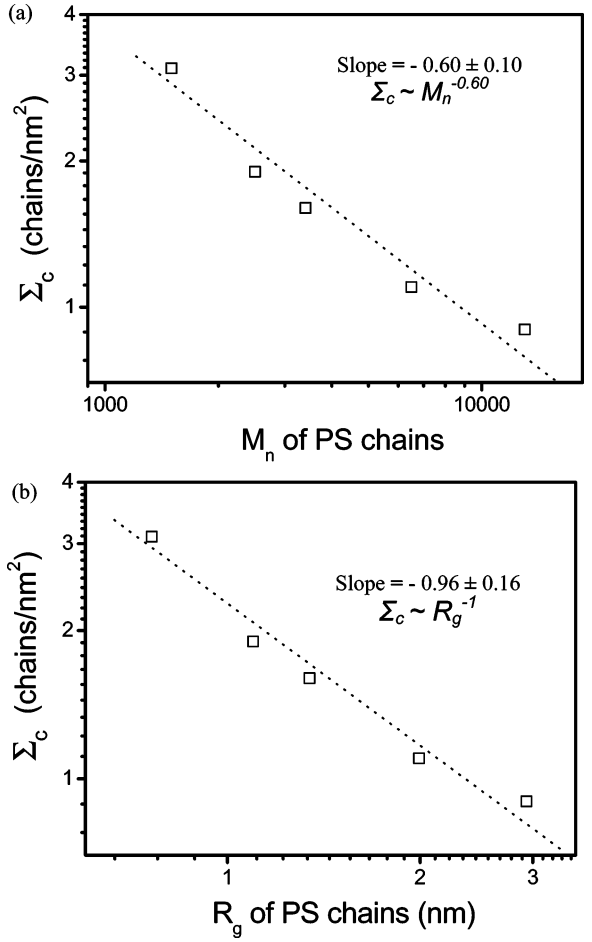

Figure 11. Critical areal chain density (Σ_C) for the transition of particle location is shown as a function of (a) the molecular weight M_n and (b) the radius of gyration R_g of PS−SH ligands, showing $\Sigma_C \sim M_n^{-0.60} \sim R_g^{-1}$. To compute the actual value for R_g of the short PS−SH chains, the wormlike chain model is used.

where h is the thickness of grafted PS shell layer. We would expect that the critical threshold for interfacial localization occurs when the areal chain density at the surface of the coated particle is itself at the mushroom to brush transition:

$$\Sigma_C' \equiv \frac{n_C}{4\pi(R+h)^2} \sim \frac{1}{R_g^2} \tag{6}$$

By plugging eq 6 into eq 3, we find

$$\Sigma_C = \Sigma_C' \frac{(R+h)^2}{R^2} \sim \frac{1}{R_g^2}\left(1+\frac{h}{R}\right)^2 \tag{7}$$

If the penetration by the PS blocks of the PS-*b*-P2VP diblock copolymers into the layer is significant so that the chains behave ideally, the layer thickness h can be estimated as $h \sim R_g$. Therefore, the critical areal density of PS brush chains to fully cover the Au particle surface can be expressed as follows:

$$\Sigma_C \sim \left(\frac{R+R_g}{R_g R}\right)^2 \tag{8}$$

Using the value of R_g of PS−SH chains and the actual mean radii of gold particles having $\Sigma \sim \Sigma_C$ coated by each different PS−SH chain, a plot of Σ_C versus $((R + R_g)/RR_g)^2$ can be constructed and is shown in Figure 12. This plot shows that Σ_C increases roughly linearly with $((R + R_g)/RR_g)^2$ but with a slope

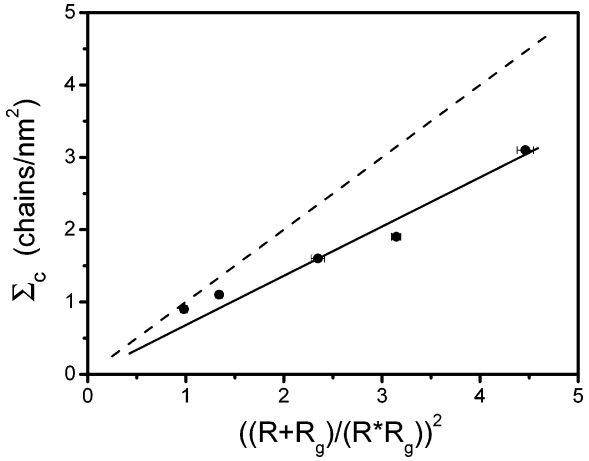

Figure 12. Critical areal chain density (Σ_C) for the transition of particle location is plotted as a function of $((R + R_g)/R_gR)^2$. The solid line represents the best fit through the origin with a slope = 0.68, while the dashed line through the origin has a slope = 1 and is shown for reference.

of about 0.68 rather than 1, i.e., critical shielding of the curved Au particle surface occurs at areal chain densities somewhat below those predicted. It is worthwhile noting that in the limit of $R \gg R_g$ the behavior of the polymer chains tethered onto the particle surface is predicted to be $\Sigma_C \sim M_n^{-1} \sim R_g^{-2}$, implying that the behavior of polymer chains on very large particles should be same as that on the flat surface. For a PS ligand of given M_n, and thus R_g, $((R + R_g)/RR_g)^2$, and thus Σ_C, decreases with increasing Au particle radius, i.e., for a given areal density of polymer ligands, the surfaces of larger, less highly curved particles will be more protected from contact with surrounding polymer chains than the surfaces of smaller, more highly curved particles. The preferential segregation of larger Au particles at the PS-*b*-P2VP interface seen in Figures 7 and 8 therefore cannot be due to their curvature but must instead be caused by an increase in their absorption energy, cf. eq 1.

Nevertheless, it should be realized that eq 8 is a very crude estimate of the critical areal chain density. To improve on this estimate, it will be worthwhile to consider more sophisticated self-consistent mean field simulations of the hybrid particle and the polymer system[49] as well as models that take into account the possibility that the thiols on the Au surface have lateral mobility and can cluster on the PS side of the PS-*b*-P2VP interface to expose bare Au to the P2VP block.[33,50]

Conclusion

We have determined the critical areal density Σ_C of PS−SH ligands on Au nanoparticles above which the PS-coated particles are predominantly in the center of the PS domain of a lamellar PS-*b*-P2VP block copolymer and below which these particles predominantly adsorb at the PS-*b*-P2VP interface. The Σ_C decreases from 3.1 to 0.9 chains/nm^2 as the M_n of PS−SH chains increases from 1.5 to 13 kg/mol, resulting in the scaling relationship $\Sigma_C \sim M_n^{-0.60}$. These results for PS chains on the particle surface are very different from those expected on a flat surface. ($\Sigma_C \sim M_n^{-1}$). A model that considers the curvature of the spherical nanoparticle accounts for the data reasonably well, producing a simple scaling relationship, $\Sigma_C \sim ((R + R_g)/RR_g)^2$ that takes into account of the high curvature of the Au nanoparticle core of radius R. For Σ close to Σ_C, some particles adsorb onto the interface while other remain in the PS domain. On average, the particles at the interface are somewhat larger, reflecting their larger adsorption energy. However, the small

number of PS−SH chains on each nanoparticle also results in large fluctuations in areal chain density from particle to particle of equal size, and these fluctuations are also of importance in determining which particles are adsorbed to the interface and which remain in the PS domain.

Appendix

Calculation of f_I. To reflect the size distribution of the gold particles coated by various PS−SH chains, the fractional weight of particles (w_i) in terms of the particle size and its fractional mean diameter $\langle A_{p,i}\rangle$ from the histogram of particle size distribution are found first. By definition, the sum of the product of these two different values gives a mean diameter $\langle A_p\rangle$ of all the fractions of particles as follows:

$$\langle A_p\rangle = \sum_i w_i\langle A_{p,i}\rangle \tag{9}$$

Therefore, the number of chains on the particle surface is

$$\langle N_i\rangle = \langle\Sigma\rangle\langle A_{p,i}\rangle \tag{10}$$

where $\langle\Sigma\rangle$ is the average value of the areal chain density. It is assumed that the fraction of particles $f(N)$ with number of chains N obeys Poisson statistics, i.e.,

$$f_i(N_i) = \exp(-\langle N_i\rangle)\frac{\langle N_i\rangle^{N_i}}{N_i!} \tag{11}$$

This equation effectively assumes that the chains attach to particles at random to produce a mean number $\langle N_i\rangle$ and a standard deviation $\sqrt{\langle N_i\rangle}$. Since the numbers N_i are small, it is easily possible to calculate $f_i(N_i)$ for any N_i. The summation of $f_i(N_i)$ from $N_i = 0$ to N_k gives the cumulative fraction of particles $F_i(N_k)$ with the number of chains equal to or less than N_k.

$$F_i(N_k) = \sum_{i=1}^{N_k} f_i(N_i) \tag{12}$$

Since $\Sigma_k = N_k/\langle A_{p,j}\rangle$, $F_i(N_k)$ can be turned into $F_i(\Sigma_k)$, which is now a function in terms of the areal chain density Σ_k. Then, the cumulative fraction of all the weight fractions of the particles ($F(\Sigma_k)$) can be expressed as follows:

$$F(\Sigma_k) = \sum_i w_i F_i(\Sigma_k) \tag{13}$$

$F(\Sigma_k)$ indicates the fraction of particles (average areal chain density $\langle\Sigma\rangle$) having an areal density equal to or less than Σ_k. With the assumption that all the particles having an areal density less than the critical areal chain density for the transition in the particle location (Σ_C) will be located at the PS/P2VP interface, $F(\Sigma_C)$ produces the fraction of particles located at the interface (f_I) at a given $\langle\Sigma\rangle$. Hence, each filled circle in panels a and b of Figure 9 represents $F(\Sigma_C)$ value at a given $\langle\Sigma\rangle$ value.

Acknowledgment. We acknowledge the support of the UCSB Materials Research Laboratory. (NSF-DMR-MRSEC Grant No. DMR05-20415). We also acknowledge our collaborators Professor Joona Bang and Professor Craig J. Hawker, whose contributions at the early stage of this research were very helpful. The help of Segyu Jang for the help in image analysis of particle size measurement is appreciated.

References and Notes

(1) Bockstaller, M. R.; Thomas, E. L. *J. Phys. Chem.* B **2003**, *107* (37), 10017−10024.
(2) Jaramillo, T. F.; Baeck, S. H.; Cuenya, B. R.; McFarland, E. W. *J. Am. Chem. Soc.* **2003**, *125* (24), 7148−7149.
(3) Bruns, N.; Tiller, J. C. *Nano Lett.* **2005**, *5* (1), 45−48.
(4) Cheng, J. Y.; Ross, C. A.; Chan, V. Z. H.; Thomas, E. L.; Lammertink, R. G. H.; Vancso, G. J. *Adv. Mater.* **2001**, *13* (15), 1174−1178.
(5) Boontongkong, Y.; Cohen, R. E. *Macromolecules* **2002**, *35* (9), 3647−3652.
(6) Kane, R. S.; Cohen, R. E.; Silbey, R. *Chem. Mater.* **1999**, *11* (1), 90−93.
(7) Lopes, W. A.; Jaeger, H. M. *Nature* **2001**, *414* (6865), 735−738.
(8) Sohn, B. H.; Seo, B. H. *Chem. Mater.* **2001**, *13* (5), 1752−1757.
(9) Spatz, J.; Mossmer, S.; Moller, M.; Kocher, M.; Neher, D.; Wegner, G. *Adv. Mater.* **1998**, *10* (6), 473−475.
(10) Bockstaller, M. R.; Lapetnikov, Y.; Margel, S.; Thomas, E. L. *J. Am. Chem. Soc.* **2003**, *125* (18), 5276−5277.
(11) Chiu, J. J.; Kim, B. J.; Kramer, E. J.; Pine, D. J. *J. Am. Chem. Soc.* **2005**, *127* (14), 5036−5037.
(12) Kim, B. J.; Chiu, J. J.; Yi, G. R.; Pine, D. J.; Kramer, E. J. *Adv. Mater.* **2005**, *17* (21), 2618−2622.
(13) Tsutsumi, K.; Funaki, Y.; Hirokawa, Y.; Hashimoto, T. *Langmuir* **1999**, *15* (16), 5200−5203.
(14) Kim, B. J.; Bang, J.; Hawker, C. J.; Kramer, E. J. *Macromolecules* **2006**, *39*, 4108−4114.
(15) Bockstaller, M. R.; Thomas, E. L. *Phys. Rev. Lett.* **2004**, *93* (16), Art. No. 166106.
(16) Corbierre, M. K.; Cameron, N. S.; Lennox, R. B. *Langmuir* **2004**, *20* (7), 2867−2873.
(17) Spontak, R. J.; Shankar, R.; Bowman, M. K.; Krishnan, A. S.; Hamersky, M. W.; Samseth, J.; Bockstaller, M. R.; Rasmussen, K. O. *Nano Lett.* **2006**, *6* (9), 2115−2120.
(18) Yeh, S. W.; Wei, K. H.; Sun, Y. S.; Jeng, U. S.; Liang, K. S. *Macromolecules* **2005**, *38* (15), 6559−6565.
(19) Kim, B. J.; Given-Beck, S.; Bang, J.; Hawker, C. J.; Kramer, E. J. *Macromolecules* **2007**, *40* (6), 1796−1798.
(20) Huang, C. M.; Wei, K. H.; Jeng, U. S.; Liang, K. S. *Macromolecules* **2007**, *40* (14), 5067−5074.
(21) Vaia, R. A.; Maguire, J. F. *Chem. Mater.* **2007**, *19* (11), 2736−2751.
(22) Brust, M.; Bethell, D.; Kiely, C. J.; Schiffrin, D. J. *Langmuir* **1998**, *14*, 5425−5429.
(23) Schmid, G.; Simon, U. *Chem. Commun.* **2005**, *6*, 697−710.
(24) Wang, S. H.; Sato, S.; Kimura, K. *Chem. Mater.* **2003**, *15*, 2445−2448.
(25) Grubbs, R. B. *Polym. Rev.* **2007**, *47* (2), 197−215.
(26) Listak, J.; Bockstaller, M. R. *Macromolecules* **2006**, *39* (17), 5820−5825.
(27) Binks, B. P. *Curr. Opin. Colloid Interface Sci.* **2002**, *7* (1−2), 21−41.
(28) Horozov, T. S.; Binks, B. P. *Angew. Chem., Int. Ed.* **2006**, *45* (5), 773−776.
(29) Xu, H.; Lask, M.; Kirkwood, J.; Fuller, G. *Langmuir* **2007**, *23* (9), 4837−4841.
(30) Stratford, K.; Adhikari, R.; Pagonabarraga, I.; Desplat, J. C.; Cates, M. E. *Science* **2005**, *309* (5744), 2198−2201.
(31) Chung, H.; Ohno, K.; Fukuda, T.; Composto, R. J. *Nano Lett.* **2005**, *5* (10), 1878−1882.
(32) Kim, B. J.; Fredrickson, G. H.; Hawker, C. J.; Kramer, E. J. *Langmuir* **2007**, *23* (14), 7804−7809.
(33) Kim, B. J.; Bang, J.; Hawker, C. J.; Chiu, J. J.; Pine, D. J.; Jang, S. G.; Yang, S. M.; Kramer, E. J. *Langmuir* **2007**, *23* (25), 12693−12703.
(34) Kunz, M. S.; Shull, K. R.; Kellock, A. J. *J. Colloid Interface Sci.* **1993**, *156* (1), 240−249.
(35) Alexander, S. *J. Phys.* **1977**, *38* (8), 983−987.
(36) Degennes, P. G. *Macromolecules* **1980**, *13* (5), 1069−1075.
(37) Brust, M.; Walker, M.; Bethell, D.; Schiffrin, D. J.; Whyman, R. *J. Chem. Soc., Chem. Commun.* **1994**, (7), 801−802.
(38) Gandubert, V. J.; Lennox, R. B. *Langmuir* **2005**, *21* (14), 6532−6539.
(39) Gittins, D. I.; Caruso, F. *Angew. Chem., Int. Ed.* **2001**, *40* (16), 3001−3004.
(40) Pryamitsyn, V.; Ganesan, V. *Macromolecules* **2006**, *39* (24), 8499−8510.
(41) Hashimoto, T.; Tanaka, H.; Hasegawa, H. *Macromolecules* **1990**, *23* (20), 4378−4386.
(42) Winey, K. I.; Thomas, E. L.; Fetters, L. J. *Macromolecules* **1992**, *25* (10), 2645−2650.
(43) Thompson, R. B.; Ginzburg, V. V.; Matsen, M. W.; Balazs, A. C. *Science* **2001**, *292* (5526), 2469−2472.

(44) Thompson, R. B.; Ginzburg, V. V.; Matsen, M. W.; Balazs, A. C. *Macromolecules* **2002**, *35* (3), 1060−1071.
(45) Chiu, J. J.; Kim, B. J.; Yi, G. R.; Bang, J.; Kramer, E. J.; Pine, D. J. *Macromolecules* **2007**, *40* (9), 3361−3365.
(46) Pieranski, P. *Phys. Rev. Lett.* **1980**, *45* (7), 569−572.
(47) Kratky, O.; Porod, G. *Recl. Trav. Chim. Pays-Bas* **1949**, *68* (12), 1106−1122.
(48) Flory, P. J. *Statistical Mechanics of Chain Molecules*; John Wiley & Sons: New York, 1969.
(49) Sides, S. W.; Kim, B. J.; Kramer, E. J.; Fredrickson, G. H. *Phys. Rev. Lett.* **2006**, *96* (25), Art. No. 250601.
(50) Shan, J.; Nuopponen, M.; Jiang, H.; Viitala, T.; Kauppinen, E.; Kontturi, K.; Tenhu, H. *Macromolecules* **2005**, *38* (7), 2918−2926.

MA701931Z